

1 Supporting Information for

2 **In-situ Grown Superhydrophobic ZIF-71 Layer Enabling Ultra-Stable Zinc Anodes for**  
3 **Long-Cycle AZBs**

4

5 Tianxu Ji<sup>a,†</sup>, Zinan Wang<sup>a,†</sup>, Peng Wang<sup>\*,a,b,c</sup>, Xiaoyu Yang<sup>a</sup>, Jihao Ye<sup>a</sup>, Xuze Tang<sup>a</sup>, Chunyan  
6 Li<sup>a,b</sup>, Yunpeng Liu<sup>d</sup>

7 <sup>a</sup>*School of Energy, Power and Mechanical Engineering, North China Electric Power*  
8 *University, Baoding, 071000, China*

9 <sup>b</sup>*Hebei Key Laboratory of Electric Machinery Health Maintenance & Failure Prevention,*  
10 *North China Electric Power University, Baoding 071003, China*

11 <sup>c</sup>*Key Laboratory of Icing and Anti/De-icing, China Aerodynamics Research and Development*  
12 *Center, Mianyang Sichuan 621000, China*

13 <sup>d</sup>*Department of Electrical Engineering, North China Electric Power University, Baoding,*  
14 *071000, China*

15 <sup>†</sup>These authors contribute equally to this paper.

16 \*Corresponding author.

17 Email: wang.peng.ncepu@foxmail.com

18

## 1 **Supplementary Experimental Section.**

### 2 **Preparation of AlVO-NMP electrode**

3 According to a reported method,  $\text{Al}_x\text{V}_2\text{O}_5 \cdot n\text{H}_2\text{O}$  was synthesized using a hydrothermal  
4 process.<sup>1</sup> Specifically, 0.364 g of  $\text{V}_2\text{O}_5$  and 2 mL of 30%  $\text{H}_2\text{O}_2$  were added to 60 mL of water  
5 under constant stirring. Once the  $\text{V}_2\text{O}_5$  dissolved, 2.414 g of  $\text{AlCl}_3 \cdot 6\text{H}_2\text{O}$  was introduced into  
6 the solution. After stirring for 0.5 h, the mixture was transferred to a polytetrafluoroethylene-  
7 lined stainless steel reactor and heated at 120 °C for 5 h. The reactor was then allowed to cool  
8 naturally to room temperature, yielding  $\text{Al}_x\text{V}_2\text{O}_5 \cdot n\text{H}_2\text{O}$ . To remove partial crystallization  
9 water, the  $\text{Al}_x\text{V}_2\text{O}_5 \cdot n\text{H}_2\text{O}$  sample was heated at 200 °C for 5 h in a vacuum drying oven. The  
10 resulting material was immersed in n-methyl-2-pyrrolidone (NMP) and subsequently filtered.  
11 After filtration, the sample was dried at 60 °C for 10 h in a vacuum drying oven to produce  
12 AlVO-NMP. A slurry was prepared by combining AlVO-NMP, Super P, and PVDF in a 7:3:1  
13 weight ratio, with NMP added to achieve the desired consistency. The mixture was thoroughly  
14 ground into a uniform paste and applied onto a 0.01 mm stainless steel mesh. Following drying  
15 at 60 °C for 24 h, the AlVO-NMP cathode was obtained, with an active material loading of  
16 about 1 mg  $\text{cm}^{-2}$ .

### 17 **Assemble symmetrical batteries and full batteries**

18 In the CR-2032 coin battery, a glass fiber with a thickness of 0.62 mm is used as the  
19 diaphragm, and 80  $\mu\text{l}$  of 1M  $\text{Zn}(\text{OTf})_2$  is used as the electrolyte. A symmetric battery ZIF-  
20 71(IS)@Zn//SZIF-71(IS)@Zn is assembled with two identical ZIF-71(IS)@Zn electrodes. Use  
21 ZIF-71(IS)@Zn@Zn as the negative electrode and AlVO-NMP as the positive electrode to  
22 assemble the complete battery ZIF-71(IS)@Zn@Zn//AlVO-NMP. The assembly method of the  
23 soft-pack symmetric battery and the soft-pack full battery is the same as that of the coin battery.

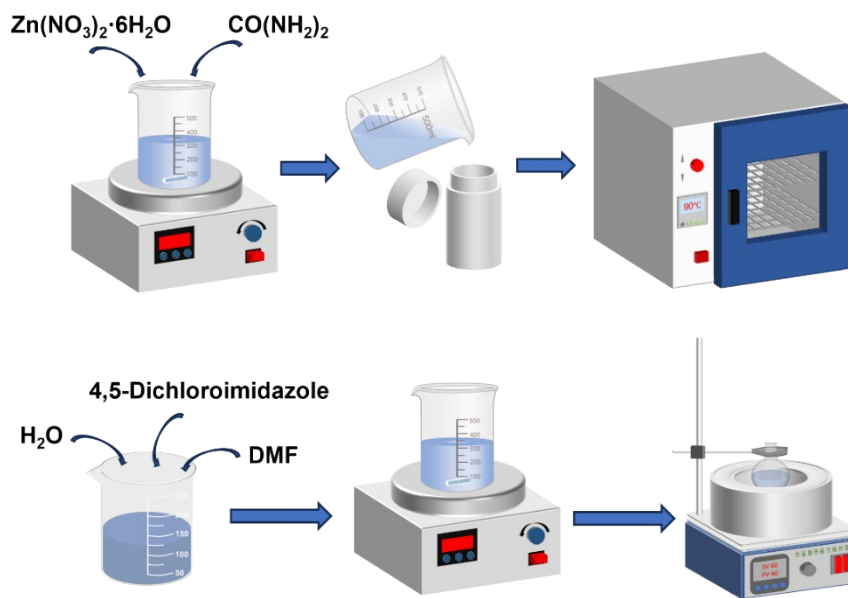
### 24 **Material characterization**

25 The surface morphology and structure of the Zn anode were examined using a scanning  
26 electron microscope (TESCAN Vega3). The chemical composition of the prepared electrode  
27 surfaces was analyzed using X-ray photoelectron spectroscopy (XPS, Thermo ESCALAB  
28 250XI, USA). X-ray diffraction (XRD) patterns were obtained with a Rigaku SmartLab SE  
29 ( $\text{Cu K}\alpha$  radiation) at a scanning rate of 2°  $\text{min}^{-1}$ . Dendrite growth was observed in situ using  
30 an optical microscope (CX-HV4800) and an in-situ cell provided by Suzhou Vision Precision  
31 Instruments Co., Ltd.

### 32 **Electrochemical measurements**

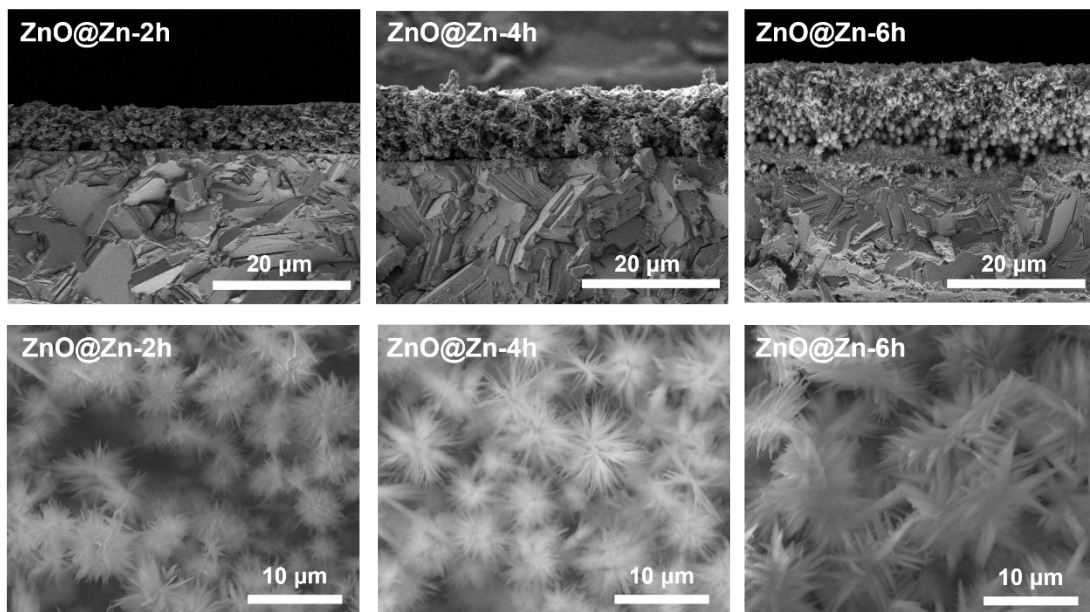
33 The electrochemical performance of half and full cells was evaluated at room temperature

1 using CR-2032 button cells and pouch cells. Constant current charge-discharge (GCD) tests  
2 were performed using the Neware Battery Test System (BTS4000, Shenzhen, China). For  
3 Zn//Cu asymmetric batteries, the charging cutoff voltage was set at 0.5 V. Additional  
4 electrochemical characterizations, including Tafel analysis, chronoamperometry (CA), linear  
5 sweep voltammetry (LSV), and electrochemical impedance spectroscopy (EIS), were carried  
6 out using the CHI 760E electrochemical workstation (Shanghai Chenhua). The open circuit  
7 voltage and internal resistance of pouch cells were measured with the HK-3560 precision  
8 internal resistance tester.



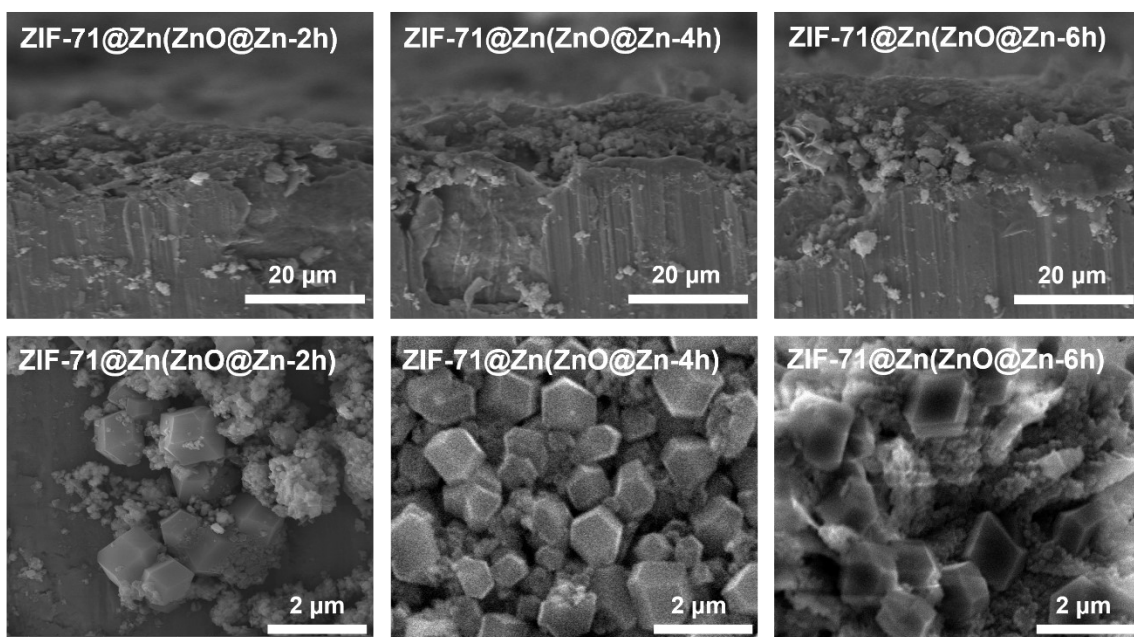
9  
10

**Fig. S1.** Preparation diagram of ZIF-71(IS)@Zn.



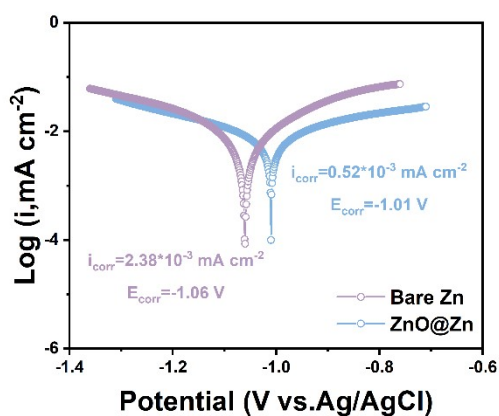
11

12 **Fig. S2.** SEM images of ZnO nanorod arrays hydrothermally grown on Zn foil for 2 h, 4 h,  
13 and 6 h at 90 °C.



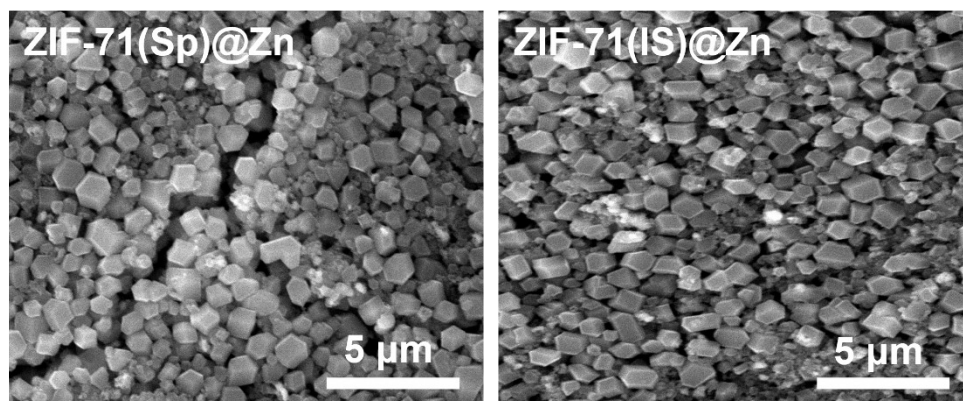
1

2 **Fig. S3.** SEM images of ZIF-71 (IS) films formed by in-situ transformation of ZnO nanorods  
 3 arrays with different initial thicknesses.



4

5 **Fig. S4.** Electrochemical Corrosion Behavior of Bare Zn and ZnO@Zn in ZIF-71 Synthesis  
 6 Solution at 75 °C.



7

8

**Fig. S5.** SEM images of ZIF-71(Sp)@Zn and ZIF-71(IS)@Zn.

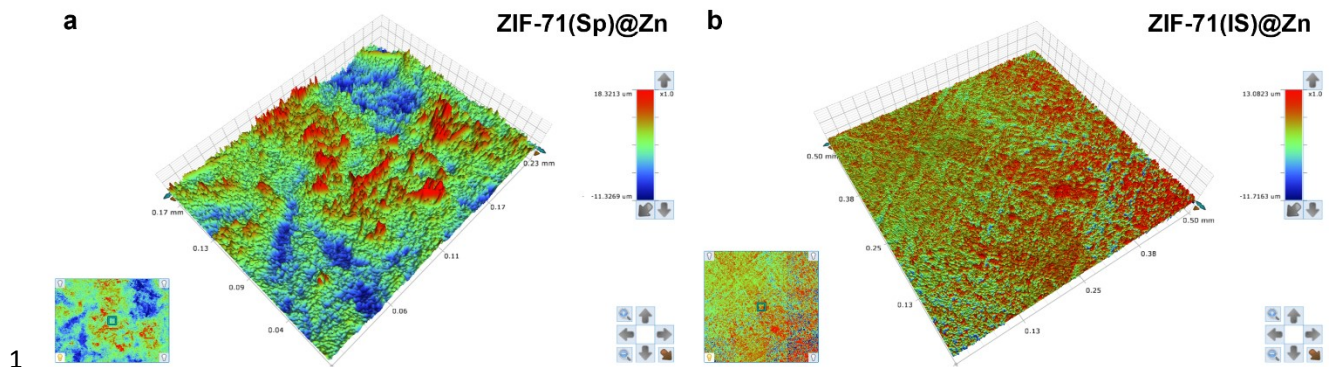


**Fig. S6.** 3D laser optical images of (a) ZIF-71(Sp)@Zn and (b) ZIF-71(IS)@Zn.

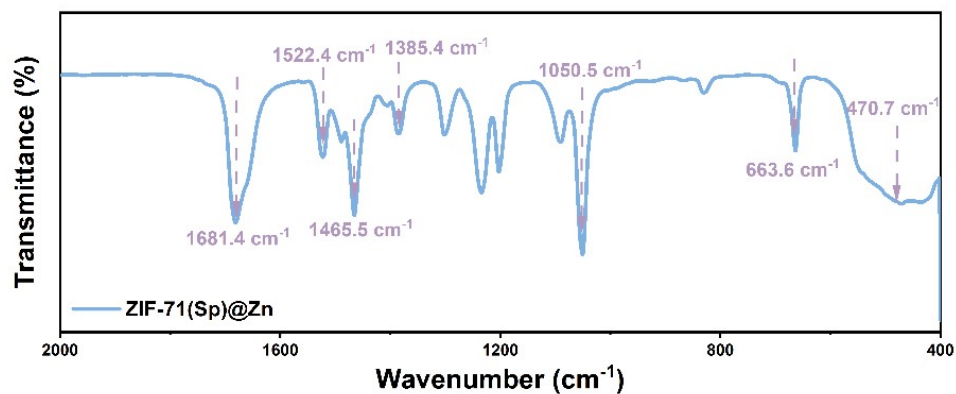


**Fig. S7.** FT-IR spectra of ZIF-71(Sp)@Zn.

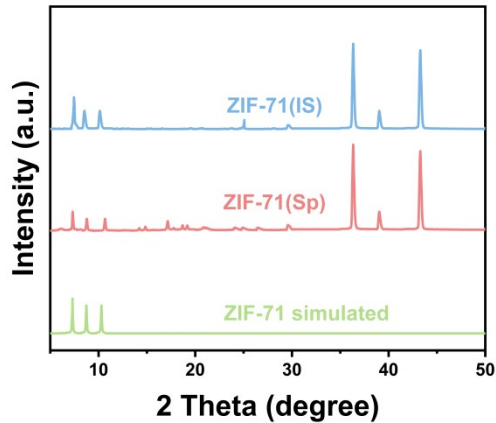
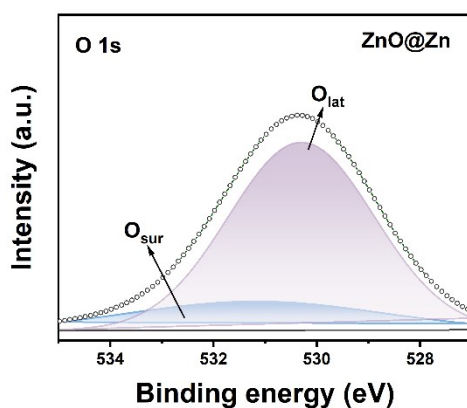


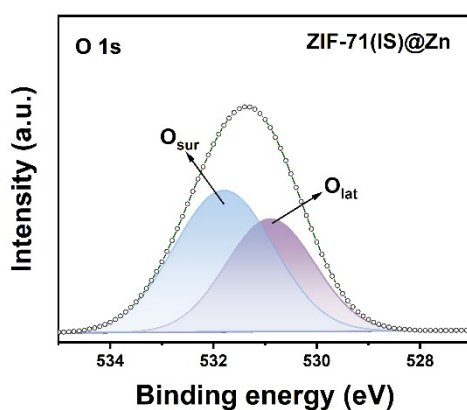
**Fig. S8.** XRD patterns of ZIF-71(IS)@Zn and ZIF-71(Sp)@Zn.



1

2

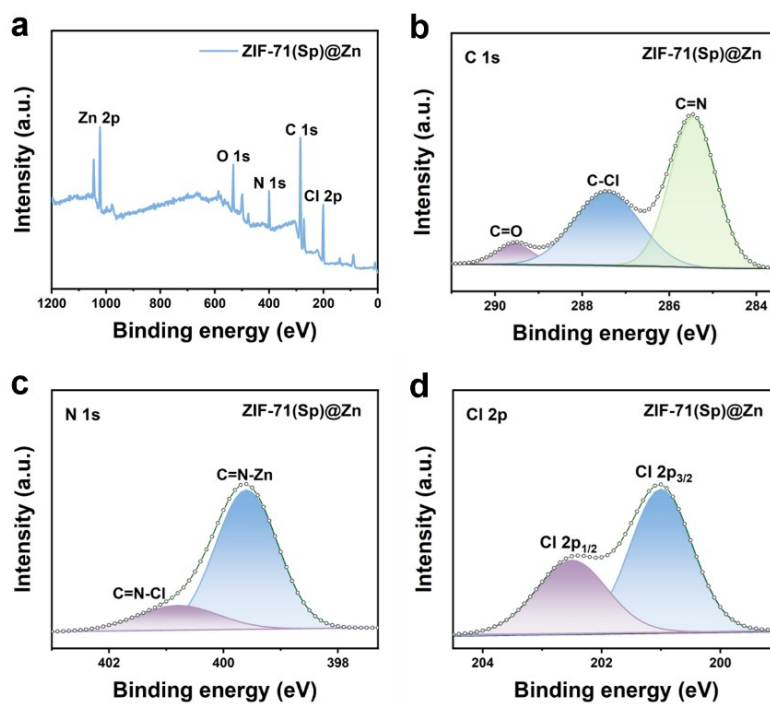
**Fig. S9.** High-resolution XPS spectrum of O 1s in ZnO@Zn.



3

4

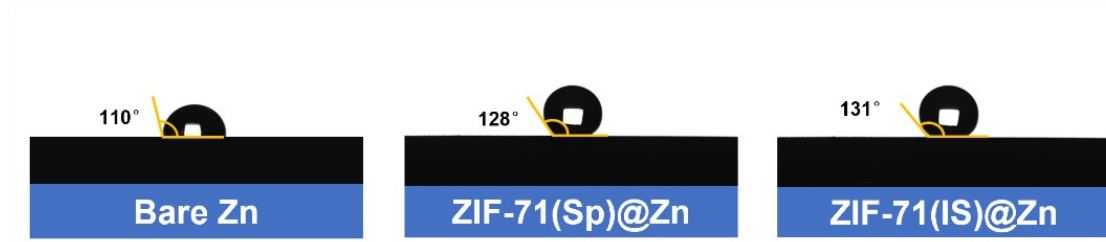
**Fig. S10.** High-resolution XPS spectrum of O 1s in ZIF-71(1S)@Zn.



5

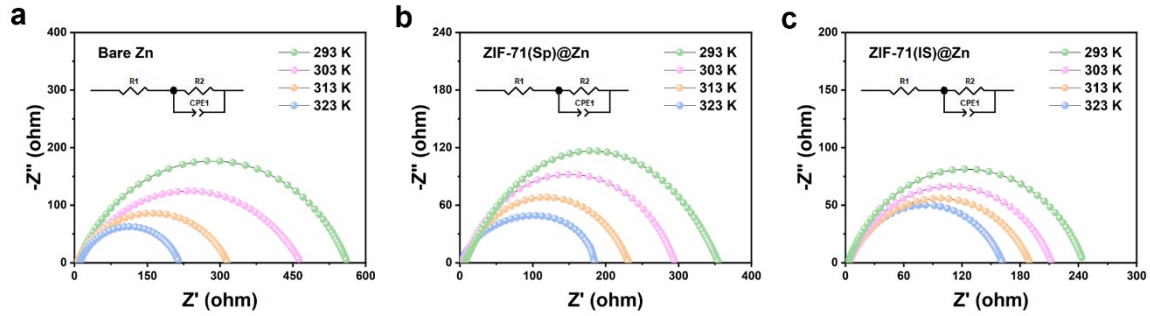
6 **Fig. S11.** (a) Full XPS spectra of ZIF-71(Sp)@Zn. High-resolution XPS spectrum of (b) C 1s,

7 (c) N 1s and (d) Cl 2p in ZIF-71(Sp)@Zn.



1

2 **Fig. S12.** Contact angles (CAs) of a  $\text{Zn}(\text{CF}_3\text{SO}_3)_2$  aqueous solution dropped on bare Zn, ZIF-  
 3 71(Sp)@Zn, and ZIF-71(IS)@Zn.



4

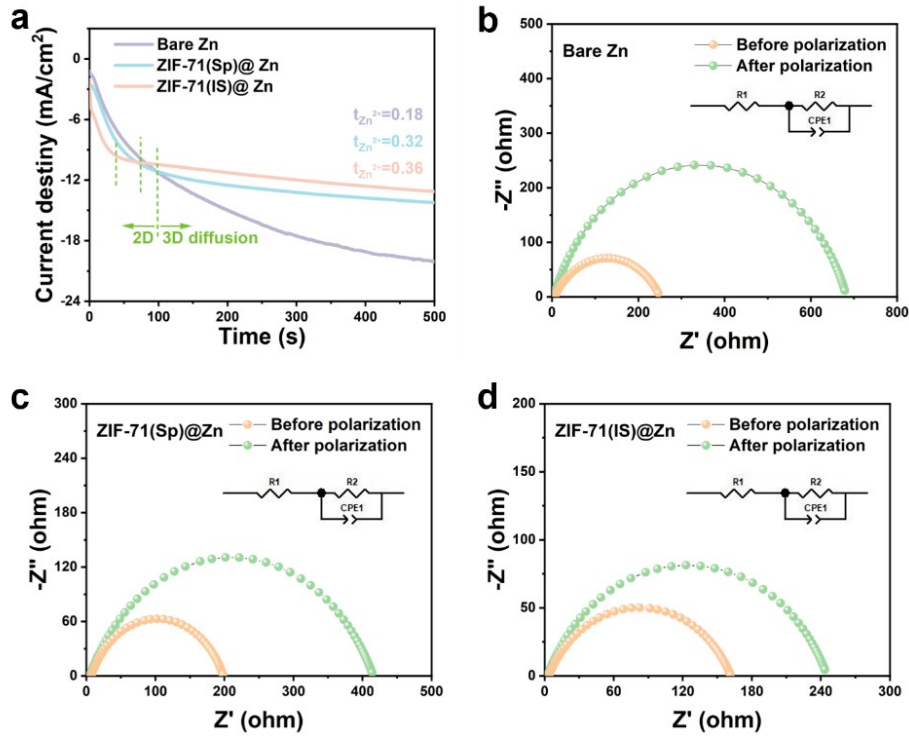
5 **Fig. S13.** Nyquist patterns at different temperatures of (a) bare Zn, (b) ZIF-71(Sp)@Zn and (c)  
 6 ZIF-71(IS)@Zn in symmetrical cells.

7 Use the Arrhenius equation (2) to calculate the activation energy ( $E_a$ ):<sup>2</sup>

8

$$\frac{1}{R_{ct}} = A \exp\left(-\frac{E_a}{RT}\right)$$

9 Here,  $R_{ct}$ ,  $A$ ,  $R$ , and  $T$  represent charge transfer resistance, frequency factor, gas constant,  
 10 and absolute temperature, respectively.



1

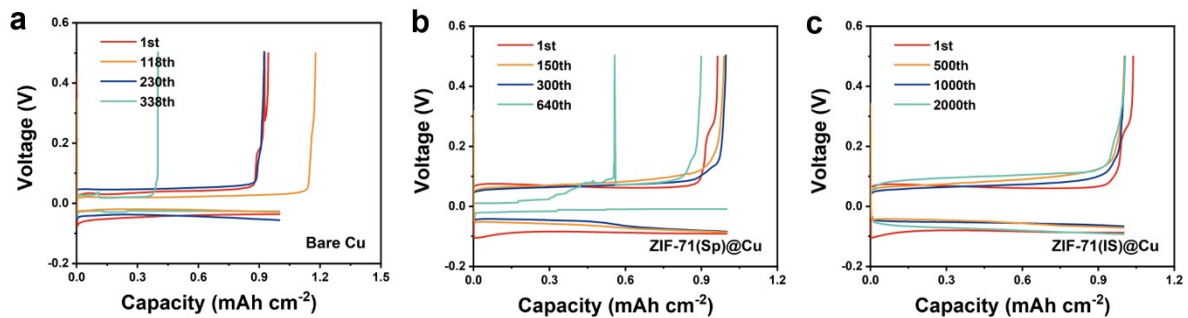
2 **Fig. S14.** (a) Chronoamperograms at a -150 mV overpotential and nyquist patterns of (b) bare  
 3 Zn, (c) ZIF-71(Sp)@Zn, ZIF-71(IS)@Zn in symmetric cells before and after polarization.

4  $Zn^{2+}$  transfer numbers ( $t_{Zn^{2+}}$ ) in the symmetric Zn cells were calculated by the Bruce-  
 5 Vincent formula (3):<sup>3</sup>

$$t_{Zn^{2+}} = \frac{I_S(\Delta V - I_0 R_0)}{I_0(\Delta V - I_S R_S)}$$

6

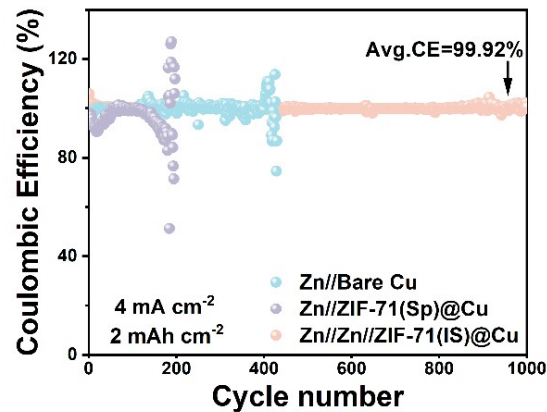
7 In this context,  $\Delta V$  represents the applied voltage polarization,  $I_S$  and  $R_S$  denote the steady-  
 8 state current and resistance, and  $I_0$  and  $R_0$  represent the initial current and resistance. The  
 9 applied polarization voltage here is -150 mV.



10

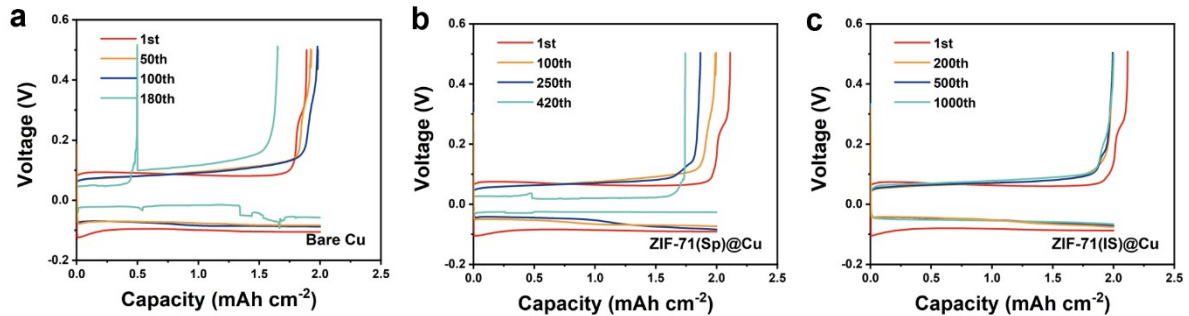
11 **Fig. S15.** Voltage profiles of (a) Zn//Cu, (b) Zn//ZIF-71(Sp)@Cu and (c) Zn// ZIF-71(IS)@Cu

1 asymmetric cells in selected cycles at  $2 \text{ mA cm}^{-2}$  (areal capacity:  $1 \text{ mAh cm}^{-2}$ ).



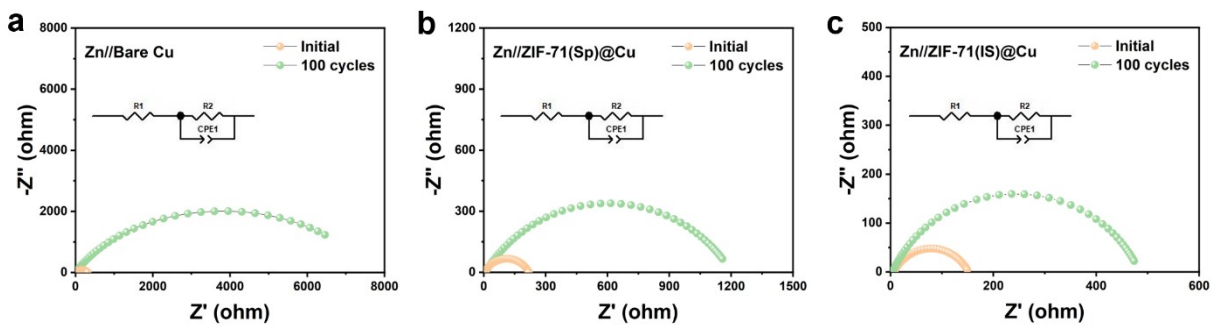
2

3 **Fig. S16.** CE of Zn plating/stripping for bare Cu, ZIF-71(Sp)@Cu and ZIF-71(IS)@Cu at 4  
4  $\text{mA cm}^{-2}$  (areal capacity:  $2 \text{ mAh cm}^{-2}$ ).



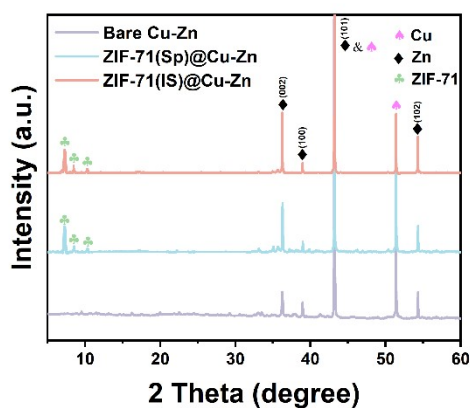
5

6 **Fig. S17.** Voltage profiles of (a) Zn//Cu, (b) Zn//ZIF-71(Sp)@Cu and (c) Zn// ZIF-71(IS)@Cu  
7 asymmetric cells in selected cycles at  $4 \text{ mA cm}^{-2}$  (areal capacity:  $2 \text{ mAh cm}^{-2}$ ).



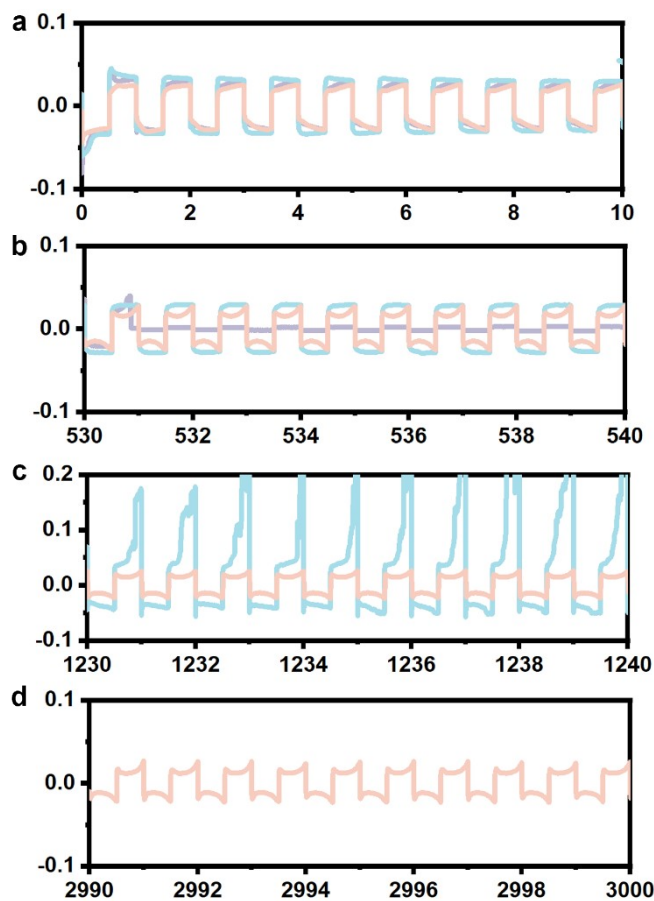
8

9 **Fig. S18.** EIS of (a) Zn//bare Cu, (b) Zn//ZIF-71(Sp)@Cu and (c) Zn//ZIF-71(IS)@Cu  
10 asymmetric cells at initial and after 100 cycles at  $4 \text{ mA cm}^{-2}$  (areal capacity:  $2 \text{ mAh cm}^{-2}$ ).



1

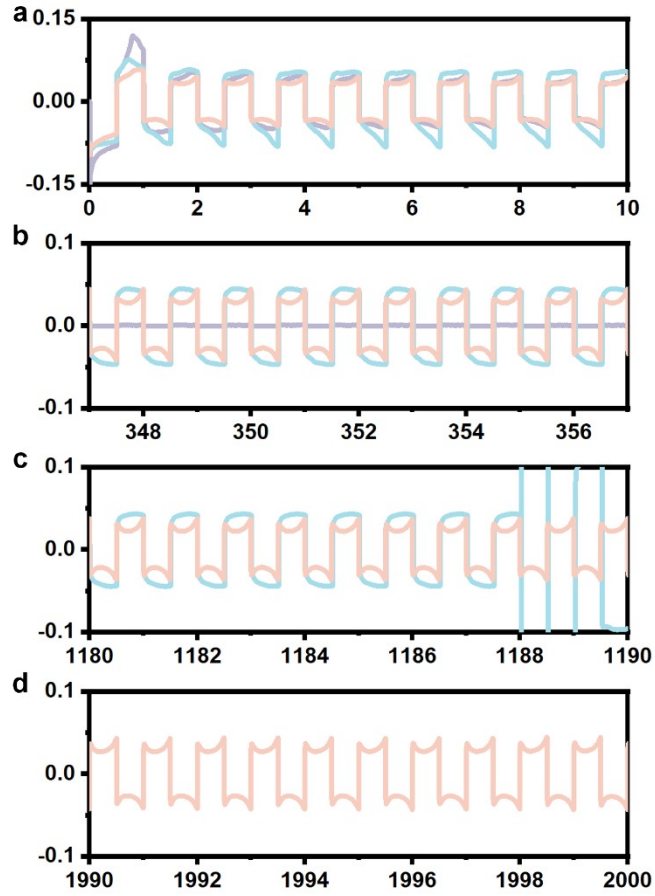
2 **Fig. S19.** XRD patterns of bare Cu, ZIF-71(Sp)@Cu and ZIF-71(IS)@Cu foils after 100 cycles  
 3 at  $4 \text{ mA cm}^{-2}$  (area capacity:  $2 \text{ mAh cm}^{-2}$ ).



4

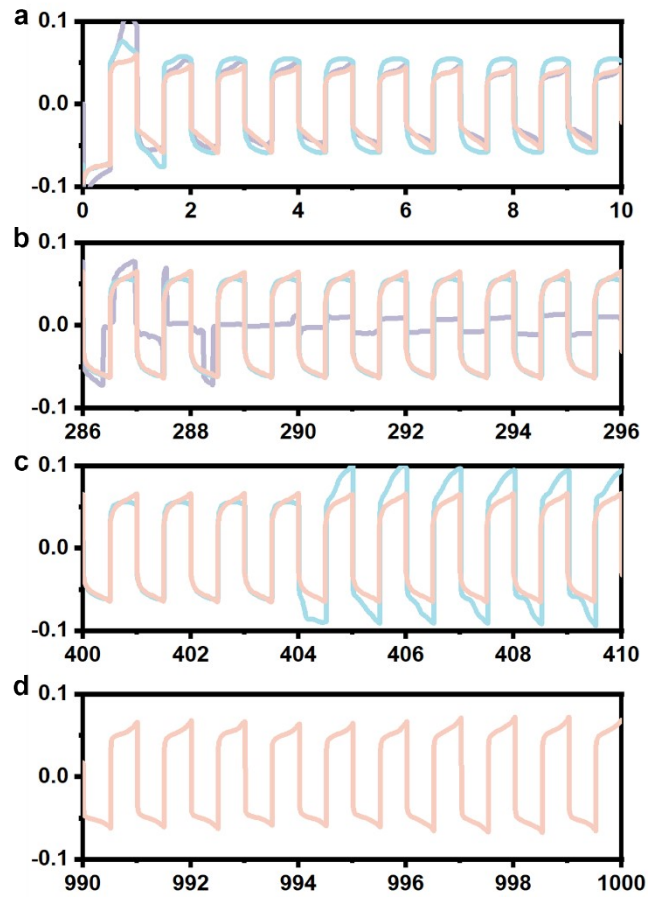
5 **Fig. S20.** Enlarged voltage profiles of bare Zn, ZIF-71(Sp)@Zn and ZIF-71(IS)@Zn  
 6 symmetric cells at  $1 \text{ mA cm}^{-2}$  during (a) 0-10 h, (b) 530-540 h, (c) 1230-1240 h and (d) 2990-  
 7 3000h.

8



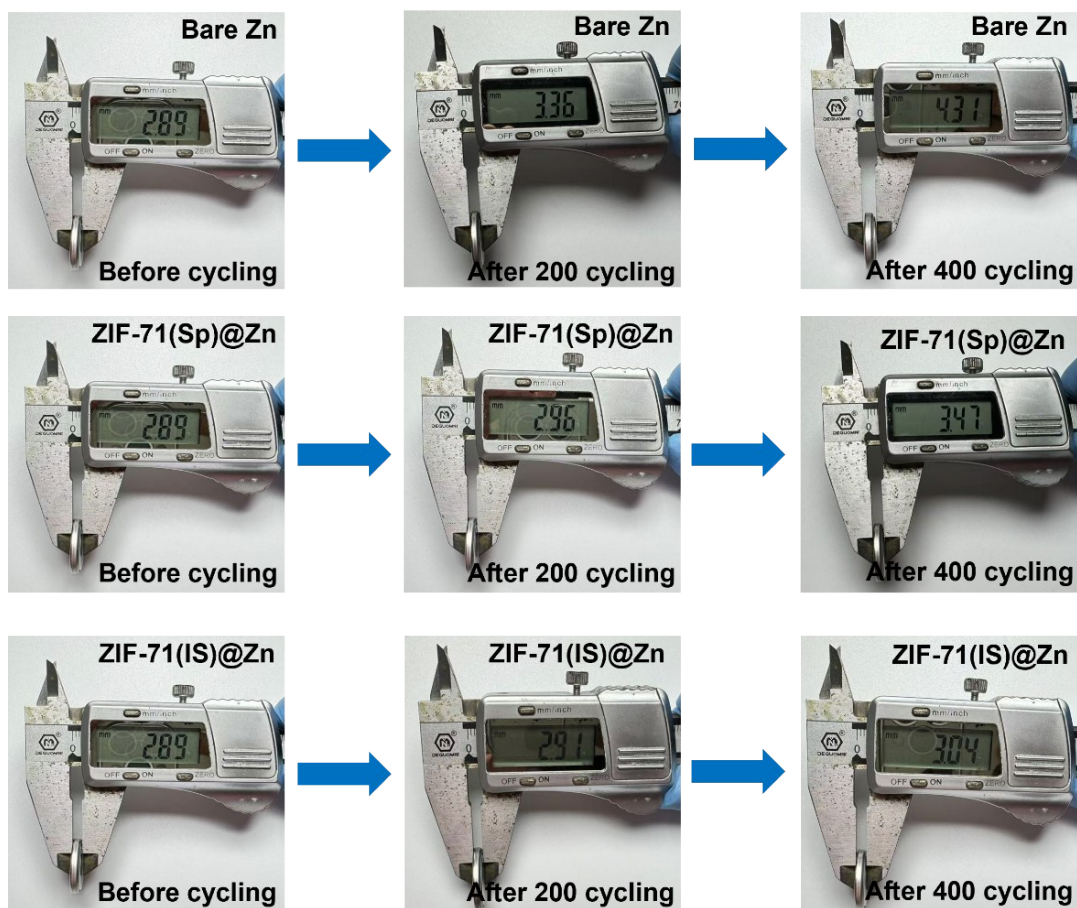
1

2 **Fig. S21.** Enlarged voltage profiles of bare Zn, ZIF-71(Sp)@Zn and ZIF-71(IS)@Zn  
 3 symmetric cells at 3 mA cm<sup>-2</sup> during (a) 0-10 h, (b) 347-357 h, (c) 1180-1190 h and (d) 1990-  
 4 2000h.



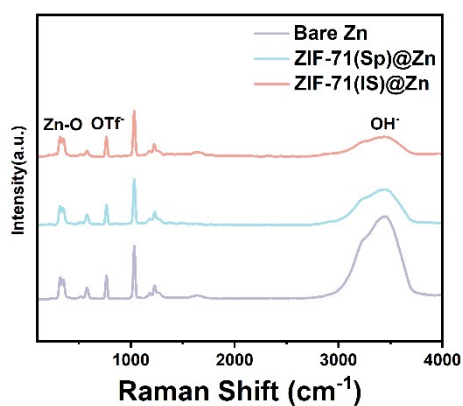
1

2 **Fig. S22.** Enlarged voltage profiles of bare Zn, ZIF-71(Sp)@Zn and ZIF-71(IS)@Zn  
 3 symmetric cells at  $4 \text{ mA cm}^{-2}$  during (a) 0-10 h, (b) 286-296 h, (c) 400-410 h and (d) 990-  
 4 1000h.



1

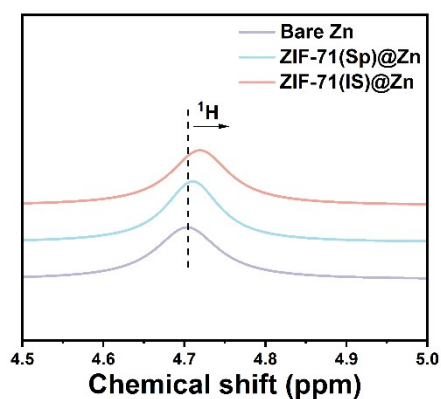
2 **Fig. S23.** Changes in thickness of bare Zn, ZIF-71(Sp)@Zn and ZIF-71(IS)@Zn button-  
 3 symmetric batteries before and after cycling at  $1 \text{ mA cm}^{-2}$  (areal capacity:  $0.5 \text{ mAh cm}^{-2}$ ).



4

5

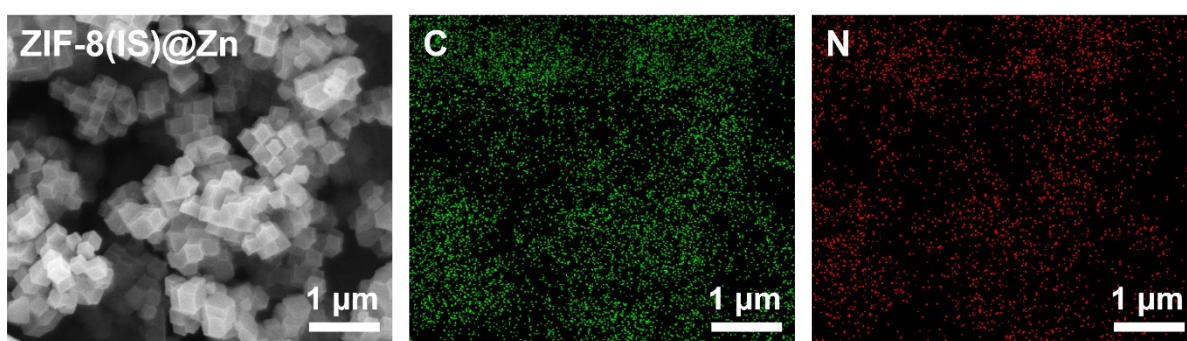
**Fig. S24.** Raman spectra of Bare Zn, ZIF-71(Sp)@Zn and ZIF-71(IS)@Zn.



1

2

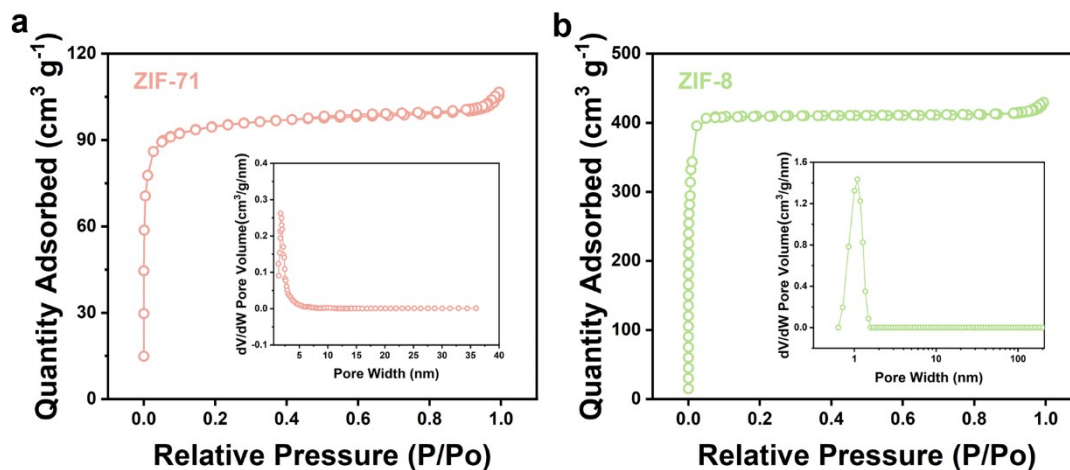
**Fig. S25.**  $^1\text{H}$  NMR spectra of Bare Zn, ZIF-71(Sp)@Zn and ZIF-71(IS)@Zn.



3

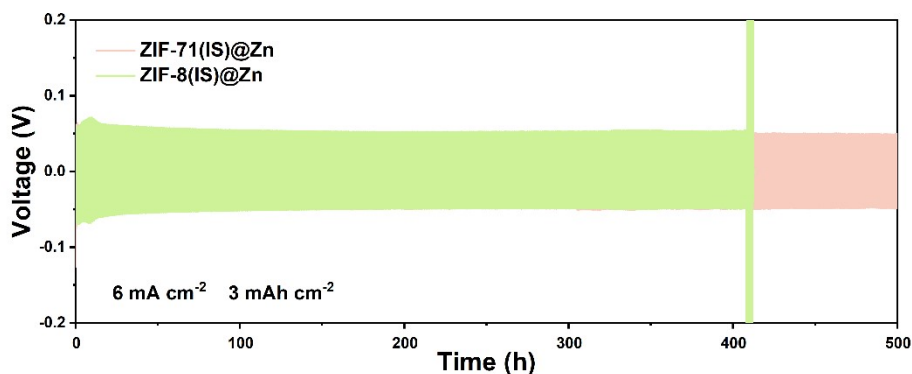
4

**Fig. S26.** SEM and EDS images of ZIF-71(IS)@Zn.



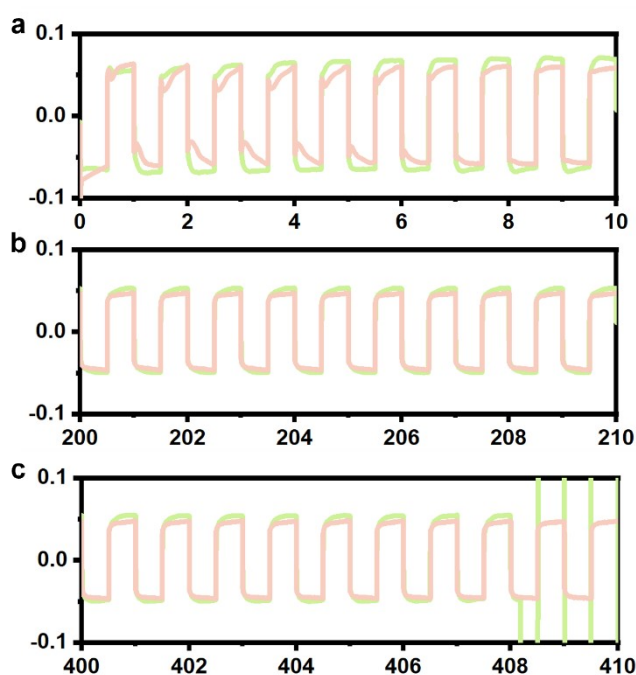
5

**Fig. S27.**  $\text{N}_2$  Adsorption/Desorption Profiles and Pore Structure Characterization of ZIF-71 and ZIF-8.



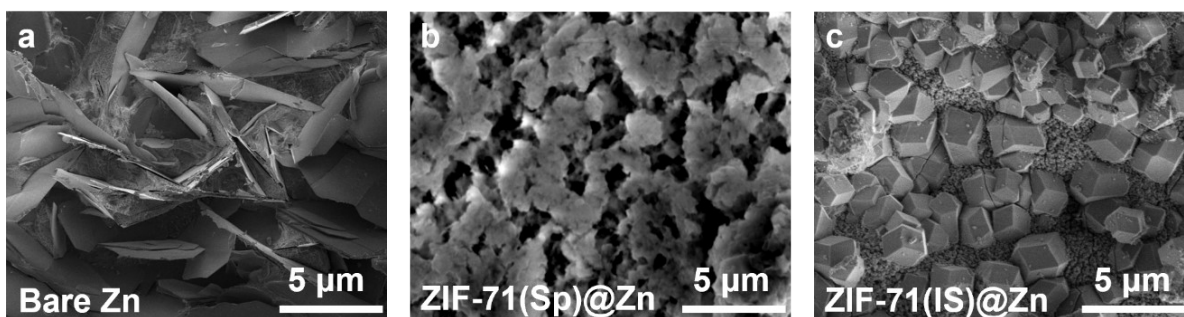
1

2 **Fig. S28.** Cycling Stability of Symmetric Cells Based on ZIF-71(IS)@Zn and ZIF-8(IS)@Zn  
 3 at  $6 \text{ mA cm}^{-2}/3 \text{ mAh cm}^{-2}$ .



4

5 **Fig. S29.** Enlarged voltage profiles of ZIF-71(IS)@Zn and ZIF-8(IS)@Zn symmetric cells at  
 6  $6 \text{ mA cm}^{-2}$  during (a) 0-10 h, (b) 200-210 h and (c) 400-410 h.

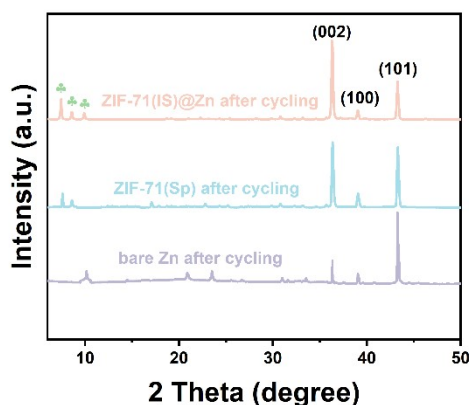


7

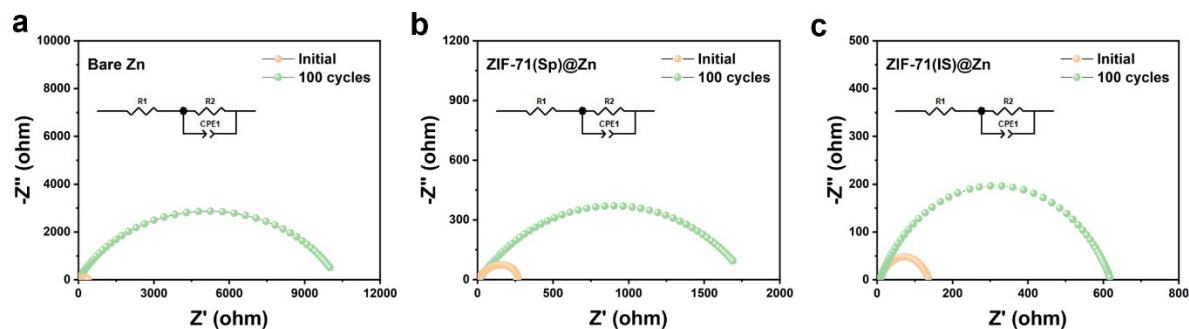
8 **Fig. S30.** SEM images showing (a) bare Zn, (b) ZIF-71(Sp)@Zn and (c) ZIF-71(IS)@Zn  
 9 following cycling for 50 h at  $3 \text{ mA cm}^{-2}$  (areal density:  $1.5 \text{ mAh cm}^{-2}$ ).



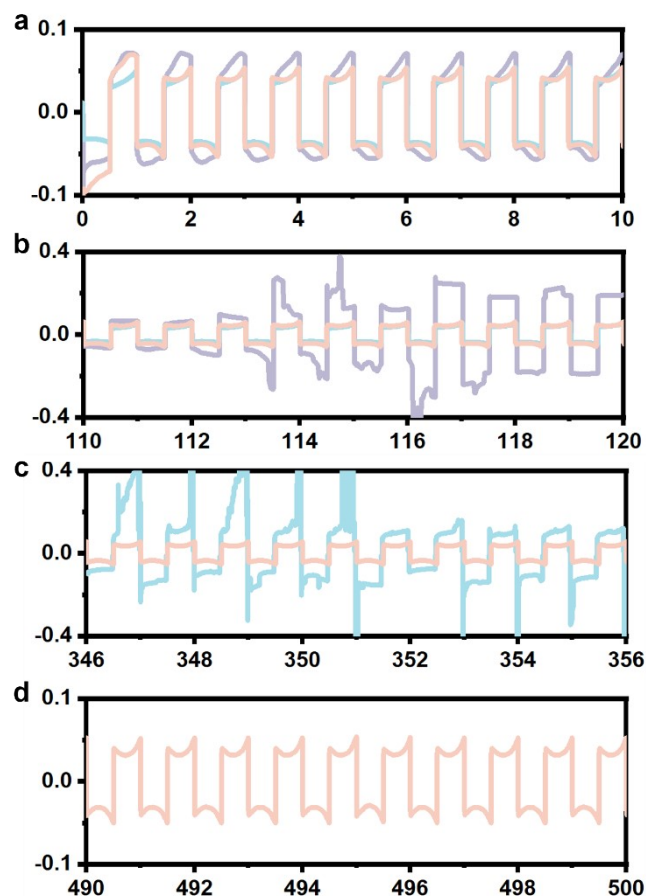
1  
2 **Fig. S31.** Images of diaphragms after 100 cycles of (a) bare Zn, (b) ZIF-71(Sp)@Zn and (c)  
3 ZIF-71(IS)@Zn symmetric cells at  $3 \text{ mA cm}^{-2}$  (areal capacity:  $1.5 \text{ mAh cm}^{-2}$ ) after 50 cycles.



4  
5 **Fig. S32.** XRD patterns of bare Zn, ZIF-71(Sp)@Zn and ZIF-71(IS)@Zn foils after 100 cycles  
6 at  $3 \text{ mA cm}^{-2}$  (area capacity:  $1.5 \text{ mAh cm}^{-2}$ ).

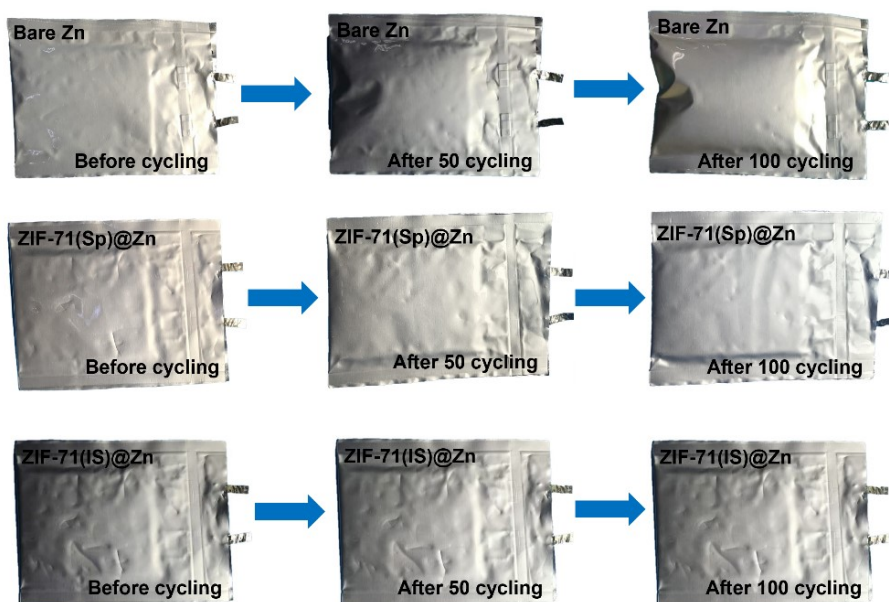


7  
8 **Fig. S33.** EIS of (a) bare Zn//bare Zn, (b) ZIF-71(Sp)@Zn//ZIF-71(Sp)@Zn and (c) ZIF-  
9 71(IS)@Zn//ZIF-71(IS)@Zn symmetric cells at initial and after 100 cycles at  $3 \text{ mA cm}^{-2}$  (areal  
10 capacity:  $1.5 \text{ mAh cm}^{-2}$ ).



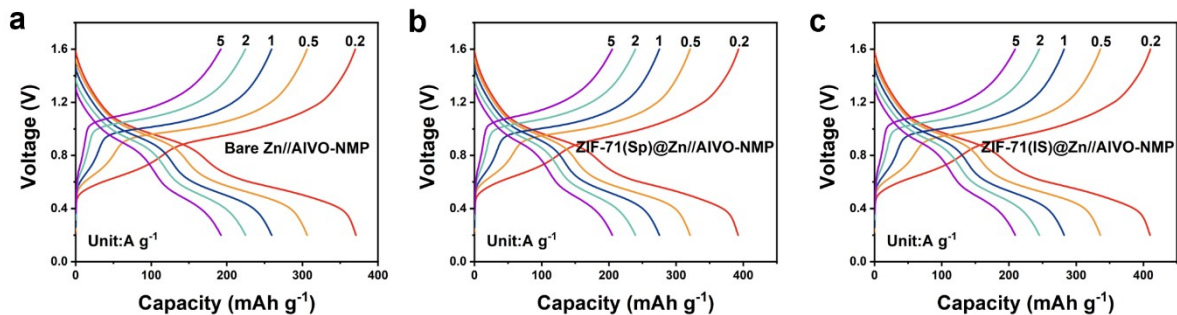
1

2 **Fig. S34.** Enlarged voltage profiles of bare Zn, ZIF-71(Sp)@Zn and ZIF-71(IS)@Zn pouch  
 3 symmetric cells at 5 mA cm<sup>-2</sup> during (a) 0-10 h, (b) 110-120 h, (c) 346-356 h and (d) 490-500h.



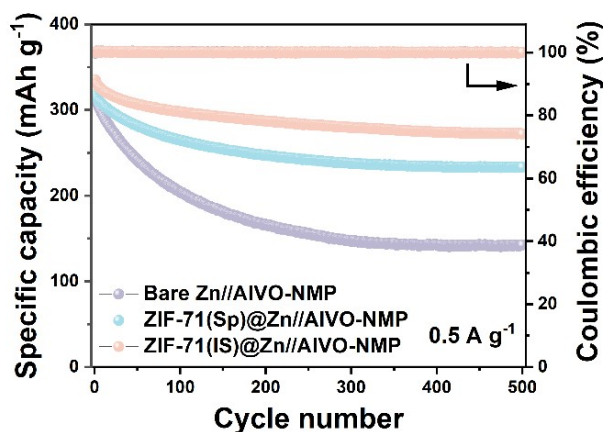
4

5 **Fig. S35.** Changes in thickness of bare Zn, ZIF-71(Sp)@Zn and ZIF-71(IS)@Zn button-  
 6 symmetric batteries before and after cycling at 2 mA cm<sup>-2</sup> (areal capacity: 1 mAh cm<sup>-2</sup>).



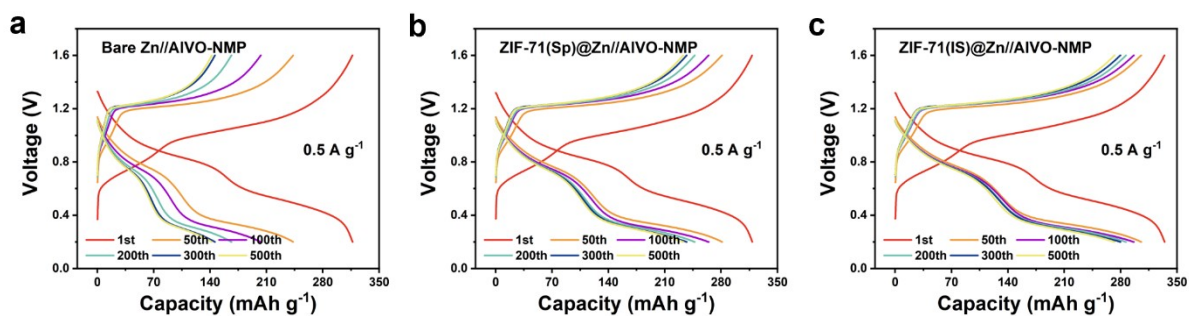
1

2 **Fig. S36.** Charge/discharge profiles of (a) bare Zn//AIVO-NMP, (b) ZIF-71(Sp)@Zn// AIVO-  
 3 NMP and (c) ZIF-71(IS)@Zn// AIVO-NMP batteries under various current densities.



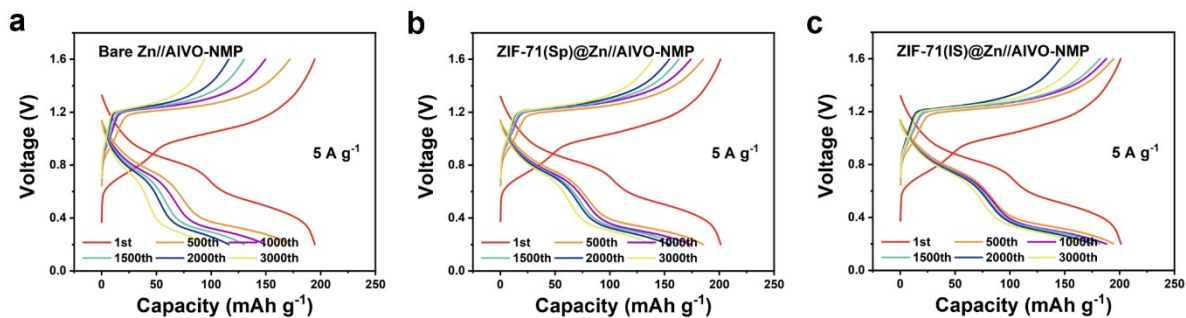
4

5 **Fig. S37.** Cycling performance of bare Zn//AIVO-NMP, ZIF-71(Sp)@Zn//AIVO-NMP and  
 6 ZIF-71(IS)@Zn//AIVO-NMP coin cells at 0.5 A g<sup>-1</sup>.



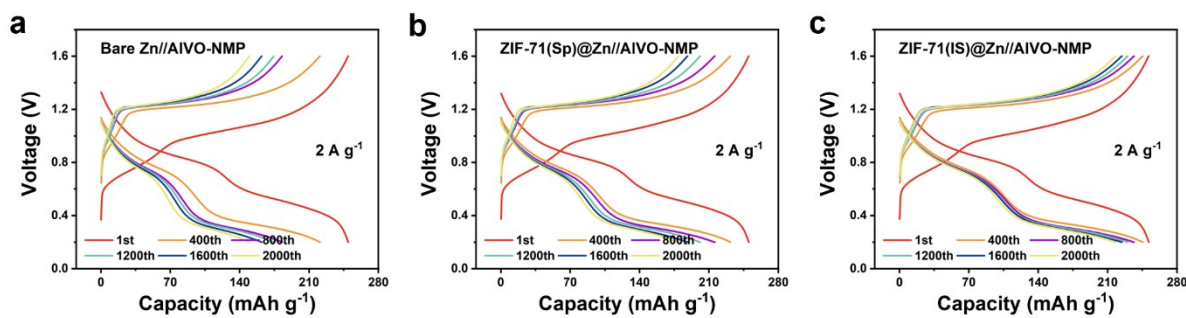
7

8 **Fig. S38.** Charge/discharge curves of (a) bare Zn//AIVO-NMP, (b) ZIF-71(Sp)@Zn// AIVO-  
 9 NMP and (c) ZIF-71(IS)@Zn// AIVO-NMP coin cells at 0.5 A g<sup>-1</sup> under selected cycles.



1

2 **Fig. S39.** Charge/discharge curves of (a) bare Zn//AIVO-NMP, (b) ZIF-71(Sp)@Zn// AIVO-  
 3 NMP and (c) ZIF-71(IS)@Zn// AIVO-NMP coin cells at 5 A g<sup>-1</sup> under selected cycles.



4

5 **Fig. S40.** Charge/discharge curves of (a) bare Zn//AIVO-NMP, (b) ZIF-71(Sp)@Zn// AIVO-  
 6 NMP and (c) ZIF-71(IS)@Zn// AIVO-NMP pouch cells at 2 A g<sup>-1</sup> under selected cycles.

7

## 1 References

- 1 F. Wan, Z. Hao, S. Wang, Y. Ni, J. Zhu, Z. Tie, S. Bi, Z. Niu and J. Chen, *Adv. Mater.*, 2021, **33**, 2102701.
- 2 Y. Feng, L. Zhou, H. Ma, Z. Wu, Q. Zhao, H. Li, K. Zhang and J. Chen, *Energy Environ. Sci.*, 2022, **15**, 1711-1759.
- 3 C. Zhao, Y. Zhang, J. Gao, Z. Guo, A. Chen, N. Liu, X. Lu, X. Zhang and N. Zhang, *Batter. Supercaps*, 2023, **6**, e202200478.

2